Appl. Chem. Eng., Vol. 27, No. 6, December 2016, 555-564
http://dx.doi.org/10.14478/ace.2016.1109

Review

메탄올 생산용 고활성 Cu/ZnO 촉매 합성방법

정천우 · 서영웅†

한양대학교 화학공학과
(2016년 11월 21일 접수, 2016년 11월 23일 심사, 2016년 11월 23일 채택)

Preparation of Active Cu/ZnO-based Catalysts for Methanol Synthesis

Cheonwoo Jeong and Young-Woong Suh†

Department of Chemical Engineering, Hanyang University, Seoul 04763, Republic of Korea
(Received November 21, 2016; Revised November 23, 2016; Accepted November 23, 2016)

초 록

대기 중 이산화탄소의 재활용 기술과 재생에너지에 의한 물 분해 기술의 접목이 최근 가능해지면서 메탄올은 많은 관심을 받고 있다. 경제성이 유리하도록 메탄올 경제를 실현하기 위해서는 고활성 메탄올 합성 촉매를 제조하여야 하며, 이를 위해서는 논리적인 접근법이 필요하다. 공침법을 통해 제조하는 Cu/ZnO 기반의 촉매는 침전, 숙성, 여과, 세척, 건조, 소성, 환원 등의 복잡한 단계로 제조되며, 100년의 역사를 가지고 있음에도 불구하고 최근에야 침전 화학과 촉매 나노구조에 대한 기초적인 이해가 이루어지고 있다. 이에 본 고에서는 단계별로 합성 변수가 침전, 소성, 환원 상태 물질의 물성에 미치는 영향에 대한 최근 결과들을 리뷰하고, 화학적 기억 효과라고 부르는 이들 물성들과 최종 촉매의 활성 사이의 관련성을 논의하였다. 제조 변수별 설명은 메탄올 합성을 위한 Cu/ZnO 기반 고활성 촉매를 제조하는 방법에 초점이 맞추어져 있다. 논의된 합성 전략은 공침법을 기반으로 하는 타 금속 또는 금속 산화물 담지 촉매의 제조에 활용 가능할 것으로 판단된다.

Abstract

In recent years, methanol has attracted much attention since it can be cleanly manufactured by the combined use of atmospheric CO_2 recycling and water splitting via renewable energy. For the concept of "methanol economy", an active methanol synthesis catalyst should be prepared in a sophisticated manner rather than by empirical optimization approach. Even though Cu/ZnO-based catalysts prepared by coprecipitation are well known and have been extensively investigated even for a century, fundamental understanding on the precipitation chemistry and catalyst nanostructure has recently been achieved due to complexity of the necessary preparation steps such as precipitation, ageing, filtering, washing, drying, calcination and reduction. Herein we review the recent reports regarding the effects of various synthesis variables in each step on the physicochemical properties of materials in precursor, calcined and reduced states. The relationship between these characteristics and the catalytic performance will also be discussed because many variables in each step strongly influence the final catalytic activity, called "chemical memory". All discussion focuses on how to prepare a highly active Cu/ZnO-based catalyst for methanol synthesis. Furthermore, the preparation strategy we deliver here would be utilized for designing other coprecipitation-derived supported metal or metal oxide catalysts.

Keywords: *methanol synthesis, Cu/ZnO, coprecipitation, chemical memory effect*

1. Introduction

Recently, George Olah, awarded a Nobel Prize in Chemistry in 1994, suggested a new concept about efficient utilization of oil and gas [1-4]. This is called "Methanol Economy", where methanol plays a central part and the products include dimethyl ether and hydrocarbons. Methanol is the smallest and easiest to store and transport as a liquid state[5]. The conventional feedstock for its manufacture is a mixture of CO, CO_2 and H_2 with small amount of CH_4 being industrially produced via incomplete combustion and reforming of fossil fuels, mainly natural gas or coal, by contact with steam or carbon dioxide in some cases[1,6-10]. Additionally, chemical recycling of CO_2 from the exhaust gases of fossil fuel-burning power plants as well as other industrial and natural sources has been realized[3,9,10]. Even atmospheric CO_2 itself can be captured and recycled through catalytic or electrochemical conversion[3,9,10-15]. This represents a chemical regenerative carbon cycle alternative to natural photosynthesis.

The methanol synthesis catalyst was developed about a century ago.

† Corresponding Author: Hanyang University,
Department of Chemical Engineering, Seoul 04763, Republic of Korea
Tel: +82-2-2220-2329 e-mail: ywsuh@hanyang.ac.kr

pISSN: 1225-0112 eISSN: 2288-4505 @ 2016 The Korean Society of Industrial and Engineering Chemistry. All rights reserved.

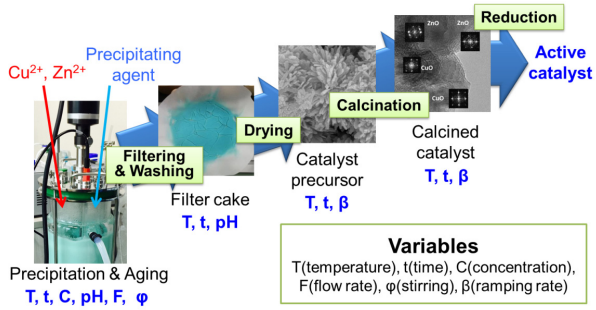

Figure 1. Overall scheme of the coprecipitation method. In each step are several variables adjusted for the production of an active Cu/ZnO-based catalyst.

In the 1920s, the catalyst composed of zinc oxide and chromium oxide was used for high-pressure methanol synthesis process, commercialized by BASF[16]. While feedstock purification, especially for sulfur removal, was the stringent challenge in 1960s, Cu-based catalysts had been studied in Imperial Chemical Industries (ICI) for the low-pressure and low-temperature process[16-20]. Finally, chromium oxide was replaced by aluminum oxide, which has been still adapted in industrial $Cu/ZnO/Al_2O_3$ catalysts.

Cu/ZnO-based catalyst is usually prepared by coprecipitation method consisting of a series of the steps such as precipitation, ageing, washing, filtering, drying, calcination and reduction as depicted in Figure 1[21]. The catalyst synthesis starts from the precipitation induced by contacting a basic precipitation agent and a mixed solution of Cu^{2+} and Zn^{2+} in a controlled manner. The next step is ageing of the precipitate that is a key for meso-structuring because the initial amorphous phase is transformed into the crystal phase accompanying color change from blue to green[22]. Prior to drying, the aged precipitate is washed and filtered repeatedly to remove anions of the metal precursor and cations of the precipitating agent (precipitant) completely. The resulting dried precipitate, usually called "precursor catalyst", shows different crystal structures depending on the Cu/Zn ratio : malachite ($Cu_2(OH)_2CO_3$), zincian malachite ($(Cu_{1-x}Zn_x)_2(OH)_2CO_3$), rosasite ($(Cu,Zn)_2(OH)_2CO_3$), aurichalcite ($(Cu_xZn_{1-x})_5(OH)_6(CO_3)_2$), and hydrozincite ($Zn_5(OH)_6(CO_3)_2$)[21,23]. The precursor catalyst is then decomposed thermally into nano-structured CuO and ZnO particles, followed by H_2 activation for producing a final Cu/ZnO-based catalyst with good Cu dispersion[21].

Consequently, the coprecipitation step is of great importance because the physicochemical properties and further catalytic performance is influenced by changing a variety of preparation variables. This is named "chemical memory effect"[16,21]. Since such variables has been determined by the empirical optimization rather than knowledge-based one, many research groups in academia have extensively tried understanding the precipitation chemistry. Herein, we review the recent progress in making a linkage between the catalytic performance and the properties of a precursor catalyst, a calcined mixed oxides and a final catalyst containing reduced Cu particles. For clarification, discussion is made step by step according to the preparation procedure, where the effect of the preparation variables on the catalytic activity is a key point in each step.

2. Step 1: Coprecipitation

The coprecipitation is simultaneous solidification of at least two different metal species upon mixing with a precipitant[16,24]. Since each metal ion would be solidified at different rates due to its ionic atmosphere, homogeneous precipitation is desired. This can be achieved successfully by adjusting many preparation variables, such as the temperature (T), time (t), metal concentration (C_M), precipitant concentration (C_P), flowrate (F), and stirring speed (φ), in an appropriate manner. All the variables except temperature affect the pH of the precipitate suspension significantly in the event of coprecipitation. Therefore, the main variables are temperature and pH in this step. Another variable we have to tune is the Cu/Zn ratio because it can determine the specific structure of precursor catalysts even though the above variables are well controlled.

2.1. Effect of the temperature

A few reports have described the effect of the temperature together with the effect of the pH in the coprecipitation. In the early study by Li and Inui, Cu/Zn/Al precursors were precipitated and subsequently aged at the same temperature[25]. The favorable precipitation occurring at the temperatures higher than 323 K (best at 343 K along with pH of 7) is explained by the presumption that a higher temperature allows the precipitation to proceed under less oversaturated conditions and thereby at a lower rate. This resulted in a more uniform precipitate where Cu and Zn were homogeneously distributed, which was evidenced by both a shift of thermal decomposition to higher temperatures for precursor catalysts and a shift of oxidation to lower temperatures for reduced catalysts. However, they concluded that the ageing temperature plays a more important role in the preparation of the precursor because the effect of the precipitation temperature became less obvious due to rearrangement of the structure during ageing.

Recently, Baltes *et al.* conducted the systematic work on finding the precipitation temperature 303-343 K and the pH 4.5-10 for the preparation of a highly active $Cu/ZnO/Al_2O_3$ catalyst containing the ration 60% Cu/30% Zn/10% Al[26]. The catalytic performance was evaluated by methanol synthesis and normalized by the activity of commercial benchmark catalyst (ICI Katalco 51-8). The best methanol productivities exceeding about 30% compared to that of the commercial catalyst were shown at neutral or a little acidic pH condition (i.e., pH 6-7) and *ca.* 343 K. These catalysts were strongly deactivated to the similar extent as the activity of commercial catalyst, thus being assumed that the commercial catalyst may be a little less active. However, the precipitation needed to be conducted at least above pH 4.5-5 and 323 K in order to synthesize an active catalyst, because the BET surface area and Cu surface area of catalysts were the lowest at low temperatures (below 323 K) and under the little acidic condition (pH 4-5). When the precipitation temperature was increased with keeping the pH lower than 5, the Cu surface area were below 5 $m^2\ g^{-1}$. However, the Cu surface area increased when both the temperature and pH were high: 24-28 $m^2\ g^{-1}$ (pH 9-10 and T > 338 K) and 25-30 $m^2\ g^{-1}$ (pH 6-7 and T > 333 K). Therefore, the coprecipitation at 333-343 K and pH 6-7

was proposed optimal for the preparation of a highly active $Cu/ZnO/Al_2O_3$ catalyst.

On the other hand, Frei *et al*. examined the influence of the precipitation and ageing temperatures in $Cu/ZnO/ZrO_2$ system for CO_2 hydrogenation[27]. Although the different crystal structures of precursor catalysts were precipitated at the temperatures between 298 and 358 K, all final $Cu/ZnO/ZrO_2$ catalysts showed the similar methanol productivity because the certain Cu/Zn/Zr precursor phase was transformed and the active catalyst was formed under their reaction condition.

2.2. Effect of the pH

Though the precipitation temperature is important as described above, controlling pH in the coprecipitation step is more crucial for the preparation of an active Cu/ZnO-based catalyst. Therefore, the precipitation behavior of metal ions is required to investigate during the process.

Behrens *et al*. conducted the titration experiments for a single metal component (Cu^{2+}, Zn^{2+} and Al^{3+}) and mixed metals as increasing the pH value relevant for precipitation[28]. In case of Cu^{2+}, a plateau was found at pH 3, which accounts for delay of the neutralization curve due to precipitation. A similar phenomenon was observed for Zn^{2+} near pH 5. When pH reaches *ca*. 11 at the end of titration experiments, tenorite (CuO) and zincite (ZnO) crystals are developed originating from the dehydration of Cu^{2+} and Zn^{2+} precipitates by bridging oxygen atoms (oxolation). In addition, olation of Al^{3+} was observed in the pH range 2.5-3.0 and the subsequent precipitation took place at pH 5 affording a colorless, amorphous precipitate (possibly aluminum hydroxide) evidenced by powder X-ray diffraction (PXRD) analysis[28-32]. Furthermore, under a very basic condition (pH 11) the major structure was dawsonite $NaAl(CO_3)(OH)_2$ and other minor crystal structures were sodium nitrate and sodium carbonates such as γ-Na_2CO_3 and $Na_2CO_3 \cdot H_2O$. When the binary Cu^{2+} and Zn^{2+} solution was titrated by a basic solution, Cu^{2+} was first precipitated at pH 3, the solution color was changed around pH 4, and then Zn^{2+} was precipitated at pH 5. This event is similarly observed for the ternary Cu^{2+}, Zn^{2+} and Al^{3+} solution, however, the hydrotalcite structure $(Cu,Zn)_{1-x}Al_x(OH)_2(CO_3)_{x/2} \cdot mH_2O$ was formed at a high pH[33].

Therefore, the pH of the precipitating suspension should be monitored for preparing an initial precipitate and further crystal structure of precursor catalyst. Practically, it can be adjusted by the method to mix each aqueous metal (acidic) and precipitating agent (basic) solutions. Hence, the precipitation process is classified into three modes, as depicted in Figure 2 : 1) addition of a precipitant solution into a metal solution (NP, normal precipitation), 2) addition of a metal solution into a basic solution (RP, reverse precipitation), and 3) simultaneous addition of both solutions thereby keeping pH constant[21,24]. The NP method is conducted in a pH-increasing mode inducing precipitation of each metal ion at different pH values. The RP method proceeds from a high to low pH leading to homogenous precipitation. The pH-constant method is achieved by a well-controlled addition of both solutions and a buffer solution. However, it is quite difficult to maintain

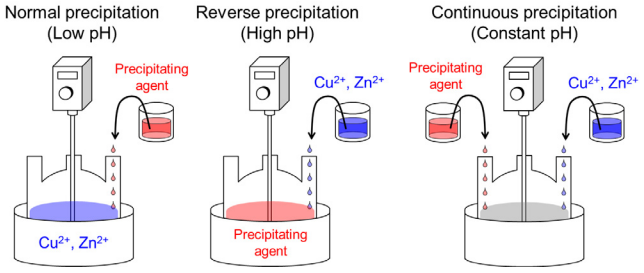

Figure 2. Coprecipitation routes: normal (addition of base to acid), reverse (addition of acid to base) and continuous (simultaneous addition of acid and base) precipitation.

the pH at a certain level during the whole precipitation process because a main control system is necessary for reading pH value continuously and, in turn, sending an output signal to feed a buffer solution at an optimal rate.

We recently reported a difference between the NP (pH-increasing mode) and RP methods (pH-decreasing mode) in the preparation of $Cu/ZnO/Al_2O_3$ catalysts with the ratio [Cu]/([Cu]+[Zn]) = 1/6, 2/4, 4/6 and 5/6 with the ratio [Al]/([Cu]+[Zn]+[Al]) fixed at 1/7[34]. The NP and RP methods produced different structures of precursor catalysts. In PXRD patterns of NP-series precursors precipitated by increasing the solution pH, several phases of hydroxycarbonate structures are shown in Figure 3 : $Cu_2(OH)_2CO_3$, $(Cu_{1-x}\ Zn_x)_2(OH)_2CO_3$, $Zn_4(OH)_6CO_3 \cdot H_2O$, and $Zn_6Al_2(OH)_{16}CO_3 \cdot H_2O$. In the Cu-rich NP precursors, all these reflections characteristic of malachite were distinctly seen with the minor reflection assigned as $Zn_6Al_2(OH)_{16}CO_3$. As the Cu/(Cu+Zn) ratio decreased, zincian malachite disappeared but the Zn-related crystal phases such as $Zn_4(OH)_6CO_3 \cdot H_2O$ and $Zn_6Al_2(OH)_{16}CO_3 \cdot 4H_2O$ became dominant. These two phases were usually observed in Cu-poor $Cu/ZnO/Al_2O_3$ precursors[35]. However, the RP precursors made by decreasing the solution pH showed very different PXRD patterns. In the Cu-rich RP precursor, zincian malachite and hydrotalcite-like $Cu_2Zn_4Al_2(OH)_{16}CO_3 \cdot 4H_2O$ (JCPDS 38-0487) were detected. The Cu-rich RP precursor displayed very intense PXRD reflections corresponding to Cu,Zn,Al hydrotalcite. In the Zn-rich RP precursors, the phase $Zn_4(OH)_6CO_3 \cdot H_2O$ became dominant, as also observed in NP precursors. The major difference between RP and NP precursors was the formation of Cu/Zn/Al hydrotalcite phase synthesized by homogeneous mixing of the three metal components, which is favorable at a high pH (i.e., RP method)[25].

The calcination of NP and RP precursors produced CuO (tenorite, JCPDS 05-0661) and ZnO (zincite, JCPDS 36-1451) though the crystal structure of each precursor was different. As the Zn content increased, the reflections of ZnO became intense and, simultaneously, the reflection intensity of CuO diminished, which is same as the results reported in the literatures[21,23]. The noticeable difference in the PXRD patterns of NP and RP mixed oxide was the peak intensity; the intensity for RP mixed oxides was less than that for NP mixed oxides. This indicates that the crystallites sizes of the former oxides are small. For the RP and NP mixed oxides with the ratio [Cu]/([Cu]+[Zn]) of 5/6, the CuO(111) crystal sizes were 6.7 and 8.9 nm, respectively.

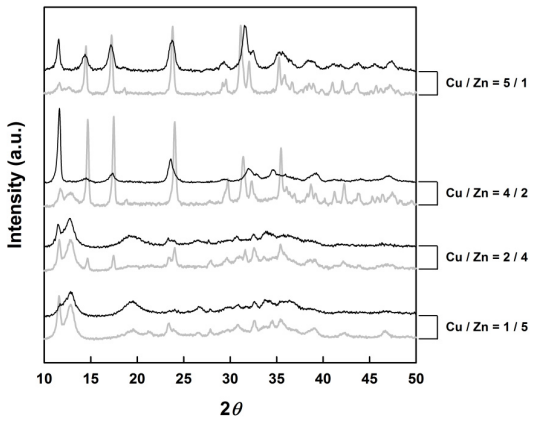

Figure 3. PXRD patterns of NP (grey) and RP (black) precursor catalysts[34].

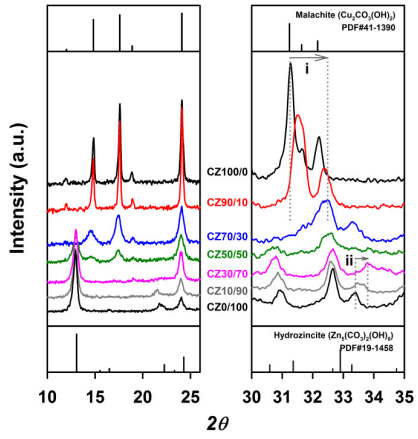

Figure 4. PXRD patterns of the Cu,Zn precursors with different Cu/Zn ratios[36].

Therefore, the RP method leads to a homogenously-mixed precursor of Cu^{2+}, Zn^{2+} and Al^{3+} and, after calcination, mixed oxide particles of small sizes. This explained a high performance of the final RP-derived $Cu/ZnO/Al_2O_3$ catalysts in the hydrogenolysis of butyl butyrate. Additionally, this work suggested a new catalyst descriptor to determine the catalytic activity (discussed later).

2.3. Effect of the Cu/Zn ratio

Even though the precipitation temperature and pH are optimized for solidification of initial precipitates, the Cu/Zn ratio is another important parameter in controlling the structural properties of precursor catalysts [21,23]. Upon precipitation of the single metal component Cu^{2+} or Zn^{2+}, the precursor structure is well defined. However, the synergy effect was found for the interim Cu/Zn ratios. We recently studied the origin of this effect by several characterization works as well as the catalytic test using the binary CuO/ZnO catalysts[36].

The PXRD reflections of CZ100/0 (Cu/Zn = 100/0) and CZ0/100 (Cu/Zn = 0/100) were identical to those of malachite and hydrozincite, respectively (Figure 4). The malachite-like reflections were observed in PXRD patterns of CZ90/10 and CZ70/30 precursors in the 2θ range 10°-26°. However, in the 2θ range 30°-35° the (20-1)-reflection of

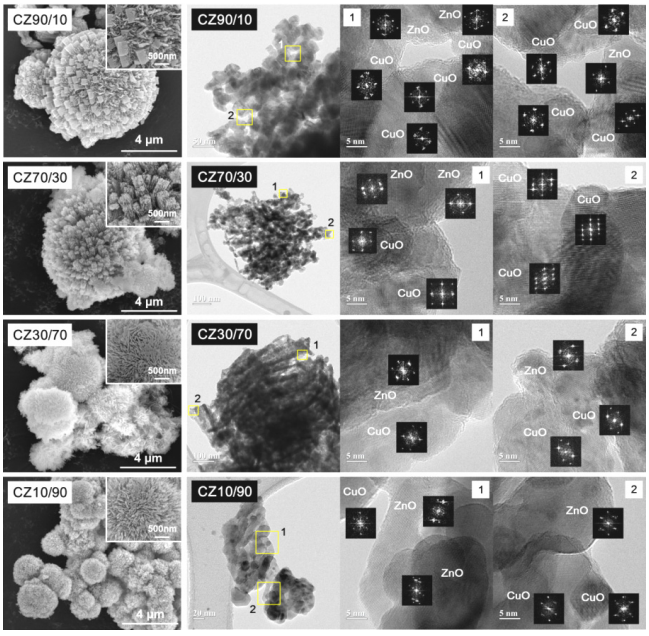

Figure 5. SEM and TEM images of the oxide samples, CZ90/10, CZ70/30, CZ30/70 and CZ10/90. Insets indicate an selected area electron diffraction pattern for the positions of CuO and ZnO letters[36].

malachite was shifted from 31.3° to 32.5° (arrow **i**), meaning that Zn^{2+} is incorporated to malachite (zincian malachite)[21,22,37]. In the Zn-rich precursors, the (002)-reflection of hydrozincite was also shifted from 33.4° to 33.8° (arrow **ii**) indicating the formation of aurichalcite by incorporation of Cu^{2+} to hydrozincite[21,37]. These incorporations were the highest in CZ70/30 and CZ30/70 precursors.

After calcination at 673 K, the morphology of CuO/ZnO mixed oxides was monitored by scanning electron microscopy (SEM) and transmission electron microscopy (TEM) as presented in Figure 5. CuO particles looked as an elongated cuboid-like surface and ZnO particles were spherical and agglomerates of platelets. For CuO/ZnO of Cu-rich, the overall morphology still kept that of CuO but some cuboid particles tended to be splitted into needles of a smaller size. For Zn-rich CuO/ZnO, the platelet-like ZnO morphology disappeared in CZ10/90 and CZ30/70 and the spherical particles looked more splitted into needles with the Cu/Zn ratio increasing. Also, HR-TEM images of CZ90/10, CZ70/30, CZ30/70 and CZ10/90 showed well intermixing of CuO and ZnO verified by the selected area electron diffraction (SAED) patterns. In contrast, a physically mixed sample was composed of isolated CuO and ZnO crystalline particles.

The well-mixed CuO/ZnO catalysts showed two types of effects compared to the physical mixture of CuO and ZnO : 1) promoting effect in Cu-rich oxides and 2) inhibiting effect in Zn-rich oxides. These effects are caused by intimate intergrowth and interfacial contact of nano-sized CuO and ZnO. Furthermore, a substitution of the second metal ion in the single crystal structure was found to affect the catalytic activity of CuO/ZnO in the decomposition of dimethylhexane-1,6-dicarbamate (HDC) to dimethylhexane-1,6-diisocyanate (HDI) for which ZnO was reported to be an active catalyst[38]. Our study re-

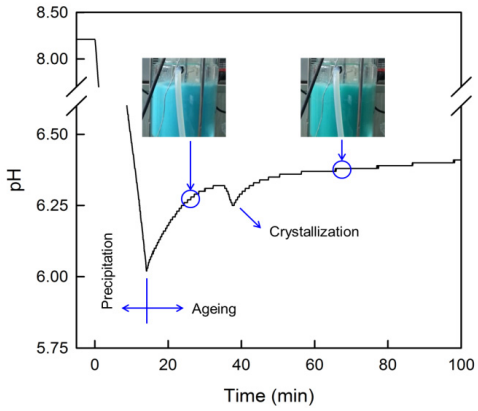

Figure 6. pH profile during the ageing of Cu,Zn precipitate.

vealed that the enhanced activity of Cu-rich mixed oxides resulted from an intimate intergrowth of nano-sized CuO and ZnO crystallites, whereas the lower activity of Zn-rich mixed oxides was due to the interfacial contact between individual CuO and ZnO nanoparticles. The similar effect was recently investigated for CuO/NiO system in Fenton-like decomposition of Bismarck Brown Y with H_2O_2[39].

3. Step 2: Ageing

The ageing is for the formation of a crystalline Cu,Zn precursor catalyst with a specific structure from an initial, amorphous precipitate [21]. The crucial synthesis parameters in the ageing step are pH, temperature (T) and time (t). Since the ageing temperature is usually identical to or a little higher than the precipitation temperature[25,26], the other variables such as the pH and time need to be carefully monitored in the ageing process.

Generally, the ageing is kept for a few hours. About 20-30 minutes after the start of ageing, the three events occurred such as a little pH drop, turbidity increase and color change from blue to green (Figure 6) [22]. These events are a result of crystallization from an amorphous to crystalline precipitate. In case of binary Cu,Zn system of Cu rich, crystalline zincian malachite was formed by the crystallization of amorphous zincian georgeite. The former phase of small crystalline needles (ca. 30-100 nm) showed the BET surface area from 32 to 57 $m^2\ g^{-1}$. Whittle *et al*. also found the similar effect of ageing for the binary precursor with the Cu/Zn ratio of 2/1[40].

Upon ageing, the structure transformation is possibly caused by complex chemical reactions such as dissolution and re-precipitation via exchanging ions[16,21,25]:

$$Cu^{2+} + 2OH^- \rightarrow [Cu(OH)_2]_s$$

$$[Cu(OH)_2]_s + Zn^{2+} + CO_3^{2-} \rightarrow [(Cu,Zn)_2(OH)_2CO_3]_s$$

$$[M(OH)_x]_s + NO_3^- \rightarrow [M(OH)_{x-1}(NO_3)]_s + OH^- \ (M = Cu^{2+} \text{ or } Zn^{2+})$$

$$[M_x(OH)_{2x-1}(NO_3)]_s + OH^- \rightarrow [M_x(OH)_{2x}]_s + NO_3^-$$

$$[M_x(OH)_{2x-1}(NO_3)]_s + H_2O \rightarrow [M_x(OH)_{2x}]_s + HNO_3$$

$$[M_x(OH)_{2x-1}(NO_3)]_s + HCO_3^- \rightarrow [M_x(OH)_{2x-1}(HCO_3)]_s + NO_3^-$$

At first, the metal ion reacts with hydroxide ions resulting in $Cu(OH)_2$ or $Zn(OH)_2$. If the mother liquor is enough acidic, some hydroxide ions in the resulting complex are replaced by nitrate ion leading to metal hydroxide nitrate (gerhardtite). When the precipitate suspension is neutral or little acidic, the metal hydroxide nitrate complex can react with water, hydroxide and bicarbonate ions. During further ageing, $Cu(OH)_2$ reacts with both Zn^{2+} and carbonate ion for the formation of $(Cu,Zn)_2(OH)_2CO_3$ complex.

In another literature, phase evolution during ageing was observed by *in-situ* energy dispersive X-ray diffraction (EDXRD)[41]. After precipitation of Cu^{2+} and Zn^{2+} by Na_2CO_3, $Na_2Zn_3(CO_3)_4 \cdot 3H_2O$ was formed as an intermediate phase. This phase then disappeared due to dissolution and was used as a source for zincian malachite[42]. If $Na_2Zn_3(CO_3)_4 \cdot 3H_2O$ is a pure Zn-phase, the initial zincian malachite should contain less Zn. In continuous ageing, Zn ions released from sodium zinc structure would be incorporated into initial zincian malachite. Such Zn replacement was examined by the shift of (20-1)-reflection of zincian malachite. Therefore, it was believed that not only crystallization of amorphous precipitates but Zn substitution in initial zincian malachite occur at the ageing step.

We recently examined the role of ZrO_2 in $Cu/ZnO/ZrO_2$ with the fixed Cu/Zn ratio of 70/30 for the ester hydrogenolysis reaction[43], though ZrO_2 is known as a promoter in Cu/ZnO-based catalysts. It has been reported that Al_2O_3 and Ga_2O_3 are substituted in a small amount into zincian malachite resulting in the enhanced catalytic performance[44-46]. In contrast, the (20-1)-reflection of zincian malachite was not shifted by addition of ZrO_2, indicating no change in the crystal structure of Cu,Zn precursor.

Therefore, we investigated the effect of ageing on Zr^{4+} incorporation into the zincian malachite lattice by comparing the morphology of the precursor CZZr-10 aged for 10 and 90 minutes (CZZr-10-10 min *vs*. CZZr-10-90 min). Large spherical particles as well as randomly dispersed small particles are shown in the TEM image of CZZr-10-10min; particularly, large particles consisted of Cu and Zn atoms whereas Zr atoms were only included in small ones (Figure 7). In the progress of ageing, large spherical particles were transformed into needles but small Zr-containing aggregates were maintained to the finish. Cu and Zn atoms were only observed in needle-like particles as marked by the arrows in the micrograph. This suggested no incorporation of Zr^{4+} in zincian malachite during ageing. Therefore, it was presumed that Zr precipitate act as a structural inhibitor like “nano-spacer”. The activity result of $Cu/ZnO/ZrO_2$ catalysts showed the volcano-type plot as a function of Zr content, where the maximum was achieved at the Zr/(Cu+Zn) ratio of 10%. This originated from nano-sized ZrO_2 that prevents sintering of CuO and Cu particles in calcined and reduced samples, respectively.

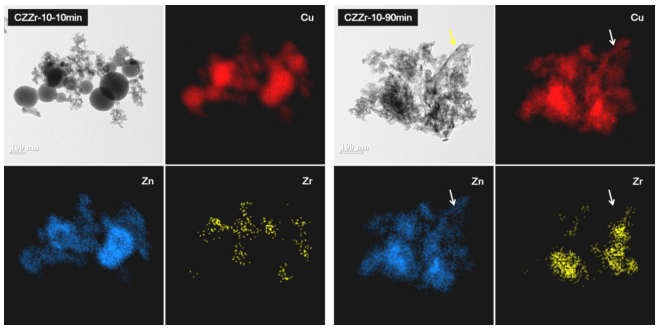

Figure 7. TEM and element mapping images of the CZZr-10 precursors recovered after ageing for 10 and 90 min. The arrows indicate Cu,Zn needles with no Zr atoms[43].

4. Step 3: Filtering and Washing

After precipitation and ageing, the anion of metal precursor and the cation of precipitating agent need to be removed by repeated filtration and washing because these ions can influence the catalytic activity. Particularly, the nitrate ion can exist as $NaNO_3$ or gerhardtite phase being known to decline the activity due to strong sintering of active Cu particles[16,21].

Bems *et al*. intensively studied the preparation and characterization of the coprecipitated Cu/ZnO catalysts[21]. It was found that the PXRD pattern of $NaNO_3$ disappeared by the first washing. However, some amounts of NO_3^- remained in the precursor catalyst. When the trace of mass 30 for NO was monitored by evolved gas analysis (EGA), the decomposition peak at 1023 K diminished and was shifted to a lower temperature as the number of washing increased. Additionally, the decomposition for CO_2 was single for the first and second washing but it happened in two steps for the further washed samples exhibiting high-temperature carbonate (HT-CO_3). It was assumed that small NO_3^- residue inhibits the formation of HT-CO_3. Also, the washing effect on the removal of sodium ion was studied as shown in Figure 8[47]. As the Na content increased up to 1.7 wt%, the methanol selectivity in CO hydrogenation was maintained and the further increase declined the methanol selectivity drastically. This means the Na ion negatively affects the catalytic activity by suppressing the synergistic effect between Cu and ZnO. Therefore, thorough washing is indispensable for an active Cu/ZnO-based catalyst.

5. Step 4: Calcination

The calcination of dried precursor is thermal phase transformation of metal hydroxycarbonate into mixed metal oxides by heating in air or O_2 atmosphere. This decomposition behavior depends mainly on the chemical structure of a precursor catalyst, which has been well documented for binary Cu,Zn precursors. The malachite (pure Cu) and hydrozincite (pure Zn) are decomposed in a single step below 673 K[21,23]:

$$Zn_5(CO_3)_2(OH)_6 \rightarrow 5ZnO + 3H_2O + 2CO_2$$

$$Cu_2(CO_3)(OH)_2 \rightarrow 2CuO + H_2O + CO_2$$

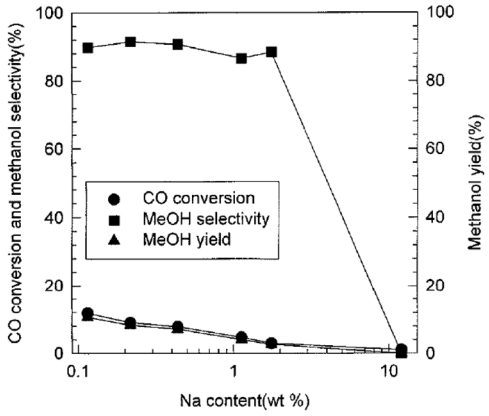

Figure 8. CO conversion, methanol selectivity and yield as a function of Na content[47].

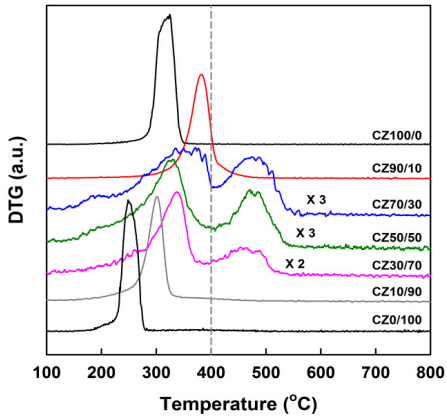

Figure 9. Derivative thermogravimetric (DTG) curves of Cu,Zn precursors with different Cu/Zn ratios[36].

$$2(Cu,Zn)_2(OH)_2CO_3 \rightarrow (Cu,Zn)_4O_3CO_3 + 2H_2O + CO_2$$

$$(Cu,Zn)_4O_3CO_3 \rightarrow 4(Cu,Zn)O + CO_2$$

For the precursors with the interim Cu/Zn ratios, two decomposition steps were visible in the range 473-673 and 673-873 K, respectively (Figure 9). The first is associated with the decomposition of pure Cu^{2+} and Zn^{2+} precursors. The second step above 673 K originated from the decomposition of HT-CO_3, the intermediate phase $(Cu,Zn)_4O_3CO_3$ transformed into mixed metal oxides[45]. This carbonate plays a role of "glue" between Cu and ZnO[21], which was observed in mineral rosasite and aurichalcite, and synthetic zincian malachite[37].

In case of ternary Cu,Zn,Zr precursors with the fixed Cu/Zn ratio of 70/30 and different Zr/(Cu+Zn) ratios, two decomposition steps were shown (Figure 10). As the content of Zr increased, the total weight loss decreased from 34.8% to 22.3% (CZZr-60, Zr/(Cu+Zn) = 60%). In the first decomposition lower than 673 K, H_2O and CO_2 were released at the same time. However, the second one above 673 K accompanied only decarbonlyation of HT-CO_3. An additional dehydroxylation event appeared in the range 373-523 K for CZZr-40 and CZZr-60 precursors. The release of lighter gas (H_2O) compared to CO_2 was the reason for the decrease of weight loss in Zr-rich precursor, meaning

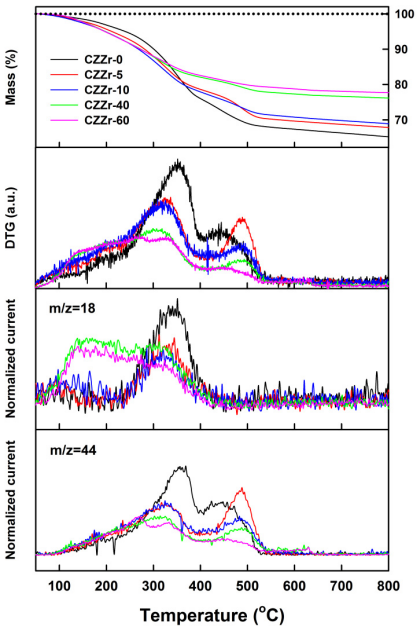

Figure 10. DTG curves of Cu,Zn,Zr precursors with different Zr/(Cu+Zn) ratios[43].

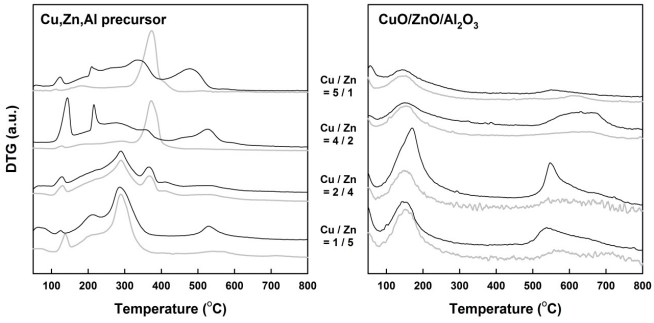

Figure 11. DTG curves of NP (grey) and RP (black) Cu,Zn,Al precursors and oxides[34].

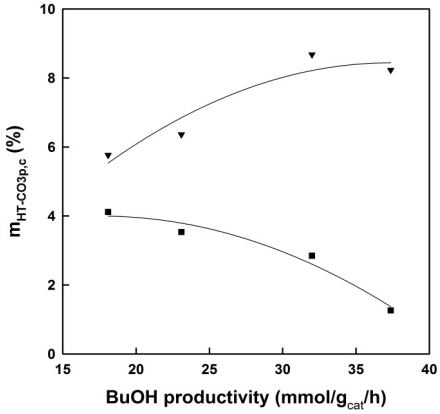

Figure 12. Correlation of $m_{HT\text{-}CO3,p}$ (▼) and $m_{HT\text{-}CO3,c}$ (■) with the butanol productivity for RP Cu/ZnO/Al_2O_3 catalysts[34].

that Zr-related phase is expected to be of OH-rich and CO_3-less structure. The weight loss of commercial $Zr(OH)_2(CO_3)\cdot ZrO_2$ was measured as 21.1% that is similar to the calculated value (20.1%) when it is supposed to be transformed into ZrO_2. Based on TG-mass results, the synthetic Zr precursor was assumed $ZrO(OH)_{2-y}(CO_3)_{y/2}$ with y of 0.18 with the accuracy in the range 0.985-1.040. This indicates that Cu/Zn/Zr precursor is a physical mixture of $(Cu_{0.7}Zn_{0.3})_2(OH)_2(CO_3)\cdot H_2O$ and $ZrO(OH)_{1.82}(CO_3)_{0.09}$ at the nominal Zr/(Cu+Zn) ratio.

In the case of Cu,Zn,Al precursors prepared by different modes (NP *vs*. RP), Cu-rich NP precursors were decomposed at *ca*. 640 K with a very large weight loss (Figure 11). This DTG peak is due to decomposition of zincian malachite confirmed by XRD results. As the precursor contained more Zn ions, the DTG peak around 560 K became more intense, which is caused by decomposition of $Zn_4(OH)_6CO_3\cdot H_2O$[23]. The decomposition of Zn-rich NP precursor was finished at 640 K because of little presence of $(Cu_{1-x}Zn_x)_2(OH)_2CO_3$[37]. Meanwhile, RP precursor showed different decomposition behavior including the existence of HT-CO_3 in the range 673-873 K[21]. This carbonate species came from two kinds of precursor such as synthetic Cu,Zn precursors and Cu,Zn,Al hydrotalcites[33,37].

In DTG curves of NP and RP CuO/ZnO/Al_2O_3 samples obtained after calcination at 673 K for 3 h, the first peak in 373-473 K corresponded to the release of water from metal oxide interlayers and the other peak in 773-973 K resulted from decarbonation of the residual HT-CO_3. The weight loss of the second decomposition was higher for RP mixed oxides than for NP ones. Also, it increased with the Cu/Zn ratio decreasing for the former samples.

When the butanol productivity was correlated with the mass loss of RP precursors ($m_{HT\text{-}CO3,p}$) and RP oxides ($m_{HT\text{-}CO3,c}$), the high performance was achieved when HT-CO_3 was abundant in precursor samples and depleted in calcined samples. It was, therefore, suggested that the amount of HT-CO_3 determines the activity of Cu/ZnO/Al_2O_3 catalyst. The pH-increasing method (NP method) induces heterogeneous precipitation because of different precipitation rates, resulting in separate crystal structures and low thermal stability of the precursor catalyst. However, the RP method, in which pH is high enough to precipitate all metal ions, leads to a mixed Cu^{2+}, Zn^{2+} and Al^{3+} precursor structure with abundant HT-CO_3, hence yielding small particles, large copper surface areas and enhanced catalytic performance. This is a consequence of chemical memory[35,48].

Aside from the metal ratio, the above thermal behavior depends on the heating condition. Schumann *et al.* studied the effect of calcination condition on HT-CO_3 of zincian malachite and aurichalcite using different heating rates in TG experiments[49]. After a little weight loss occurred at low temperatures due to water desorption, HT-CO_3 was decomposed at *ca*. 700 K. When the ramping rate was slowest at 0.1 K min^{-1}, the calcined oxide contained the highest amount of HT-CO_3 (weight loss of about 8%). With the ramping rate increasing to 2 K min^{-1}, the residual fraction of HT-CO_3 decreased to 3% in both precursor phases. The zincian malachite derived catalysts showed better methanol productivity in an initial period, but they were rapidly deactivated. Meanwhile, the aurichalcite derived catalysts produced less methanol and the deactivation rate was little less. It was weakly mentioned that the

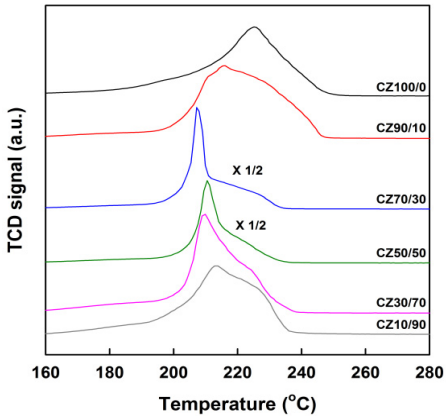

Figure 13. TPR profiles of CuO/ZnO samples with different Cu/Zn ratios[36].

HT-CO_3 abundant catalyst prepared by slow heating showed less catalytic performance, which is similar to our previous report[34]. In addition, Tarasov *et al*. suggested the four-step competitive reaction model via a thermokinetic approach[50]. Therefore, controlling the calcination condition is necessary for the preparation of an active Cu/ZnO-based catalyst since thermal decomposition behavior is quite complex.

6. Step 5: Reduction

Prior to the reaction, CuO/ZnO-based catalyst should be reduced to Cu/ZnO-based one, accompanying H_2 consumption and concomitant evolution of H_2O and CO_2[49]. In this transformation would be changed CuO reduction, mobility of CuO and ZnO, and particle morphology. Among the properties of the reduced catalyst, the principal catalytic descriptor is Cu surface area measured by N_2O titration or reactive frontal chromatography (RFC).

Investigation of this step usually starts from a temperature-programmed reduction (TPR) experiment. The reduction behavior is mainly affected by the Cu/Zn ratio. Even though a linear relationship was found between H_2 consumption with the Cu/(Cu+Zn) ratio, the reduction temperature (T_{max}) was influenced by the interaction between CuO and ZnO[36]. While the Cu/(Cu+Zn) ratio decreased from pure Cu or increased from pure Zn, T_{max} was similarly shifted to lower temperatures (Figure 13). It was explained by the fact that CuO particles became smaller in Cu-rich oxides compared to pure CuO while the interaction of CuO with ZnO was stronger in Zn-rich oxides[51,52]. Therefore, this low-temperature shift was believed to result from intermix and interfacial contact of CuO and ZnO nanoparticles.

When H_2 reduction is conducted at high temperatures, CuO and ZnO can be transformed into CuZn alloy phase[53-55]. For example, the formed α-brass showed a decrease in the BET surface area and a strong negative influence in the water-gas shift reaction[53]. The bulk mobility of Cu particles is also related with the reduction temperature because bulk re-crystallization of Cu is expected to start from 678 K, that is, the Tammann temperature of Cu. Therefore, the reduction temperature would be selected carefully for an active Cu/Zn-based catalyst.

Upon H_2 reduction, the catalyst morphology is known to be restructured[56-58]. The observation was done by *in-situ* TEM experiments under different gas conditions[46,57,59]. Under the oxidizing gas condition, Cu-related particles were spherical-like. However, they were transformed into flat shape and the *b*/*a* ratio of Wulff circle decreased due to strong metal support interaction (SMSI) under the reducing gas condition[46,58]. These findings were later confirmed at an atomic scale[57].

As for CuO, ZnO can be partially reduced into ZnO_x in the reduction step. Recently, Lunkenbein *et al*. reported the presence of ZnO_x in the reduced Cu/ZnO/Al_2O_3 catalyst by TEM[59]. Under a reduction condition, graphite-like ZnO was formed, which is metastable and distorted. Longer exposure to irradiating electron beam modified the structural morphology into three parts. At first, ZnO started to overgrow and cover the Cu particle surface. Then, ZnO crystallized into metastable rock-salt, followed by the formation of thermodynamically stable wurtzite-type ZnO after further beam irradiation.

Recent works revealed that the specific copper surface area obtained by N_2O titration could not be identical to the number of exposed Cu surface atoms because of oxidation of the partially reduced Zn species by N_2O[60,61]. Nevertheless, the copper surface area measured using N_2O gas has been still recognized as the best indicator for the catalytic performance of Cu/ZnO-based catalysts.

7. Concluding Remarks

For the preparation of a highly active Cu/ZnO-based catalyst, several experimental variables should be tuned carefully in the five preparation steps such as the precipitation, ageing, filtering and washing, calcination, and reduction. The most important is the first step of coprecipitation in which pH is the principal variable to be monitored and then adjusted. Although the three modes for mixing an acidic metal solution and a basic precipitant solution are reported, the suspension would be neutral or little acidic in the pH range 6-7 during precipitation process in order to result in homogeneous precipitation. Meanwhile, the precipitation temperature should be maintained in 333-343 K. In the next ageing step, the condition to transform initial, amorphous precipitate into a specific crystalline phase would be required. While the temperature and pH for ageing are usually identical to those for precipitation, one have to notice a few signals, such as pH drop, turbidity and color change, accompanied by the crystallization event. The aged precipitate should be washed thoroughly to remove activity inhibiting components, which is the only concern in the washing step. The so-obtained metal hydroxycarbonate phase will be transformed into mixed oxide particles and further to Cu/ZnO particles by thermal treatment steps such as calcination in air or O_2 and subsequent reduction in H_2. In case of calcination, high-temperature carbonate species acting as glue between particles would be burned in a controlled manner without sintering. The final step is H_2 reduction below Tammann temperature of Cu metal, thus resulting in higher specific Cu surface area with partially reduced ZnO_x surface related to SMSI effect.

Consequently, careful tuning of various preparation variables is in-

dispensable for promoting the key properties of a final Cu/ZnO-based catalyst: Cu surface area, Cu defect sites and ZnO SMSI. This is indeed "chemical memory" effect, which is to be considered for preparation of a final catalyst achieving superior methanol synthesis performance. Although discussion is made for Cu/ZnO-based catalysts, the synthesis strategy we reviewed herein can be applied in a similar way for preparation of other coprecipitated catalysts with metals or metal oxides supported.

Acknowledgments

The authors are grateful for financial support by C1 Gas Refinery Program and Basic Science Research Program through the National Research Foundation of Korea (NRF) funded by the Ministry of Science, ICT & Future Planning (NRF-2015M3D3A1A01064905) and by the Ministry of Education (NRF-2016R1A6A1A03013422), respectively.

References

1. G. A. Olah, A. Goeppert, and G. K. S. Prakash, *Beyond Oil and Gas: The Methanol Economy,* 2nd ed., 1-10, Wiley-VCH, Weinheim, Germany (2009).
2. G. A. Olah, Beyond oil and gas: The methanol economy, *Angew. Chem. Int. Ed.*, **44**, 2636-2639 (2005).
3. G. A. Olah, A. Goeppert, and G. K. S. Prakash, Chemical recycling of carbon dioxide to methanol and dimethyl ether: From greenhouse gas to renewable, environmentally carbon neutral fuels and synthetic hydrocarbons, *J. Org. Chem.*, **74**, 487-498 (2009).
4. *Methanol economy*, https://en.wikipedia.org/wiki/Methanol_economy, 14th November 2016.
5. J. Ott, V. Gronemann, F. Pontzen, E. Fiedler, G. Grossmann, D. B. Kersebohm, G. Weiss, and C. Witte, *Ullmann's Encyclopedia of Industrial Chemistry*, Methanol, 1-27, Wiley-VCH, Weinheim, Germany (2012).
6. R. Schlögl, The revolution continues: Energiewende 2.0, *Angew. Chem. Int. Ed*., **54**, 4436-4439 (2015).
7. X.-M. Liu, G. Q. Lu, Z.-F. Yan, and J. Beltramini, Recent advances in catalysts for methanol synthesis via hydrogenation of CO and CO_2, *Ind. Eng. Chem. Res.*, **42**, 6518-6530 (2003).
8. J.-P. Lange, Methanol synthesis: a short review of technology improvements, *Catal. Today*, **64**, 3-8 (2001).
9. S. G. Jadhav, P. D. Vaidya, B. M. Bhanage, and J. B. Joshi, Catalytic carbon dioxide hydrogenation to methanol: A review of recent studies, *Chem. Eng. Res. Des.*, **92**, 2557-2567 (2014).
10. W. Wang, S. Wang, X. Ma, and J. Gong, Recent advances in catalytic hydrogenation of carbon dioxide, *Chem. Soc. Rev.*, **40**, 3703-3727 (2011).
11. E. E. Barton, D. M. Rampulla, and A. B. Bocarsly, Selective solar-driven reduction of CO_2 to methanol using a catalyzed p-GaP based photoelectrochemical Cell, *J. Am. Chem. Soc.*, **130**, 6342-6344 (2008).
12. W.-H. Wang, Y. Himeda, J. T. Muckerman, G. F. Manbeck, and E. Fujita, CO_2 hydrogenation to formate and methanol as an alternative to photo- and electrochemical CO_2 reduction, *Chem. Rev.*, **115**, 12936-12973 (2015).
13. J. Zhang, *Electrochemical Reduction of Carbon Dioxide: Fundamentals and Technologies*, 1-45, CRC Press, USA (2016).
14. D. Nazimek and B. Czech, Artificial photosynthesis-CO_2 towards methanol, *IOP Conf. Ser.: Mater. Sci. Eng.*, **19**, 012010 (2010).
15. M. Watanabe, Photosynthesis of methanol and methane from CO_2 and H_2O molecules on a ZnO surface, *Surf. Sci. Lett.*, **279**, L236-L242 (1992).
16. K. P. de Jong, *Synthesis of Solid Catalysts,* 329-351, Wiley-VCH, Weinheim (2009).
17. G. Lormand, Industrial production of synthetic methanol, *Ind. Eng. Chem.,* **17**, 430-432 (1925).
18. Per K. Frolich, M. R. Fenske, and D. Quiggle, Catalysts for the formation of alcohols from carbon monoxide and hydrogen, *Ind. Eng. Chem.*, **20**, 694-698 (1928).
19. M. R. Fenske and Per K. Frolich, Catalysts for the formation of alcohols from carbon monoxide and hydrogen, *Ind. Eng. Chem.*, **21**, 1052-1055 (1929).
20. D. Cornthwaite, Methanol synthesis catalyst, *US Patent 3,923,694* (1975).
21. B. Bems, M. Schur, A. Dassenoy, H. Junkes, D. Herein, and R. Schlögl, Relations between synthesis and microstructural properties of copper/zinc hydroxycarbonates, *Chem. Eur. J.*, **9**, 2039-2052 (2003).
22. M. Behrens, Meso- and nano-structuring of industrial Cu/ZnO/(Al_2O_3) catalysts, *J. Catal.*, **267**, 24-29 (2009).
23. G. J. Millar, I. H. Holm, P. J. R. Uwins, and J. Drennan, Characterization of precursors to methanol synthesis catalysts Cu/ZnO system, *J. Chem. Soc., Faraday Trans.*, **94**, 593-600 (1998).
24. G. Ertl, H. Knözinger, F. Schüth, and J. Weitkamp, *Handbook of Heterogeneous Catalysis,* 100-119, Wiley-VCH, Weinheim, Germany (2008).
25. J.-L. Li and T. Inui, Characterization of precursors of methanol synthesis catalysts, copper/zinc/aluminum oxides, precipitated at different pHs and temperatures, *Appl. Catal. A*, **137**, 105-117 (1996).
26. C. Baltes, S. Vukojević, and F. Schüth, Correlations between synthesis, precursor, and catalyst structure and activity of a large set of CuO/ZnO/Al_2O_3 catalysts for methanol synthesis, *J. Catal.*, **258**, 334-344 (2008).
27. E. Frei, A. Schaadt, T. Ludwig, H. Hillebrecht, and I. Krossing, The influence of the precipitation/ageing temperature on a Cu/ZnO/ZrO_2 catalyst for methanol synthesis from H_2 and CO_2, *ChemCatChem*, **6**, 1721-1730 (2014).
28. M. Behrens, D. Brennecke, F. Girgsdies, S. Kißner, A. Trunschke, N. Nasrudin, S. Zakaria, N. F. Idris, S. B. A. Hamid, B. Kniep, R. Fischer, W. Busser, M. Muhler, and R. Schlögl, Understanding the complexity of a catalyst synthesis: Co-precipitation of mixed Cu,Zn,Al hydroxycarbonate precursors for Cu/ZnO/Al_2O_3 catalysts investigated by titration experiments, *Appl. Catal. A*, **392**, 93-102 (2011).
29. C. C. Perry and K. L. Shafran, The systematic study of aluminium speciation in medium concentrated aqueous solutions, *J. Inorg. Biochem.*, **87**, 115-124 (2001).
30. A. C. Vermeulen, J. W. Geus, R. J. Stol, and P. L. de Bruyn, Hydrolysis-precipitation studies of aluminum (III) solutions. 1. Titration of acidified aluminum nitrate solutions, *J. Colloid Interface Sci.*, **51**, 449-458 (1975).
31. B. C. Faust, W. B. Labiosa, K. H. Dai, J. S. MacFall, B. A. Browne, A. A. Ribeiro, and D. D. Richter, Speciation of aqueous mononuclear Al(III)-hydroxo and other Al(III) complexes at concentrations of geochemical relevance by aluminum-27 nuclear

magnetic resonance spectroscopy, *Geochim. Cosmochim. Acta*, **59**, 2651-2661 (1995).
32. S. L. Wang, M. K. Wang, and Y. M. Tzou, Effect of temperatures on formation and transformation of hydrolytic aluminum in aqueous solutions, *Colloids Surf. A*, **231**, 143-157 (2003).
33. M. Behrens, I. Kasatkin, S. Kühl, and G. Weinberg, Phase-pure Cu,Zn,Al hydrotalcite-like materials as precursors for copper rich $Cu/ZnO/Al_2O_3$ catalysts, *Chem. Mater.*, **22**, 386-397 (2010).
34. C. Jeong, J. Park, J. W. Bae, and Y.-W. Suh, Comparison of normal and reverse precipitation methods in the preparation of $Cu/ZnO/Al_2O_3$ catalysts for hydrogenolysis of butyl butyrate, *Catal. Commun.*, **54**, 1-5 (2014).
35. C. Busetto, G. Del Piero, and G. Manara, Catalysts for low-temperature methanol synthesis: Preparation of Cu-Zn-Al mixed oxides via hydrotalcite-like precursors, *Chem. Mater.*, **22**, 386-397 (2010).
36. C. Jeong, M. J. Hyun, and Y.-W. Suh, Activity of coprecipitated CuO/ZnO catalysts in the decomposition of dimethylhexane-1,6-dicarbamate, *Catal. Commun.*, **70**, 34-39 (2015).
37. M. Behrens, F. Girgsdies, A. Trunschke, and R. Schlögl, Minerals as model compounds for Cu/ZnO catalyst precursors: Structural and thermal properties and IR spectra of mineral and synthetic (zincian) malachite, rosasite and aurichalcite and a catalyst precursor mixture, *Eur. J. Inorg. Chem.*, 2009, 1347-1357 (2009).
38. M. J. Hyun, M. Shin, Y. J. Kim, and Y.-W. Suh, Phosgene-free decomposition of dimethylhexane-1,6-dicarbamate over Zn.O, *Res. Chem. Intermed.*, **42**, 57-70 (2016).
39. K. F. Ortega, A. Hüttner, J. Heese, and M. Berhens, Effect of Ni incorporation into malachite precursors on the catalytic properties of the resulting nanostructured CuO/NiO catalysts, *Eur. J. Inorg. Chem.*, 2016, 2063-2071 (2016).
40. D. M. Whittle, A. A. Mirzaei, J. S. J. Hargreaves, R. W. Joyner, C. J. Kiely, S. H. Taylor, and G. J. Hutchings, Co-precipitated copper zinc oxide catalysts for ambient temperature carbon monoxide oxidation: effect of precipitate ageing on catalyst activity, *Phys. Chem. Chem. Phys.*, **4**, 5915-5920 (2002).
41. S. Zander, B. Seidlhofer, and M. Behrens, In situ EDXRD study of the chemistry of aging of co-precipitated mixed Cu,Zn hydroxycarbonates - consequences for the preparation of Cu/ZnO catalysts, *Dalton Trans.*, **41**, 13413-13422 (2012).
42. T. E. Gier, X. Bu, S.-L. Wang, and G. D. Stucky, $Na_2Zn_3(CO_3)_4 \cdot 3H_2O$, a microporous sodium zincocarbonate with a diamond-type tetrahedral-triangular topology, *J. Am. Chem. Soc.*, **118**, 3039-3040 (1996).
43. C. Jeong and Y.-W. Suh, Role of ZrO_2 in $Cu/ZnO/ZrO_2$ catalysts prepared from the precipitated Cu/Zn/Zr precursors, *Catal. Today*, **265**, 254-263 (2016).
44. M. Behrens, S. Zander, P. Kurr, N. Jacobsen, J. Senker, G. Koch, T. Ressler, R. W. Fischer, and R. Schlögl, Performance improvement of nanocatalysts by promoter-induced defects in the support material: Methanol synthesis over Cu/ZnO:Al, *J. Am. Chem. Soc.*, **135**, 6061-6068 (2013).
45. J. Schumann, T. Lunkenbein, A. Tarasov, N. Thomas, R. Schlögl, and M. Behrens, Synthesis and Characterisation of a Highly Active Cu/ZnO:Al Catalyst, *ChemCatChem*, **6**, 2889-2897 (2014).
46. J. Schumann, M. Eichelbaum, T. Lunkenbein, N. Thomas, M. Consuelo, Á. Galván, R. Schlögl, and M. Behrens, Promoting strong metal support interaction: Doping ZnO for enhanced activity of Cu/ZnO:M (M = Al, Ga, Mg) catalysts, *ACS Catal.*, **5**, 3260-3270 (2015).
47. Y.-W. Suh and H.-K. Rhee, Optimum washing conditions for the preparation of $Cu/ZnO/ZrO_2$ for methanol synthesis from CO hydrogenation: Effects of residual sodium, *Korean J. Chem. Eng.*, **19**, 17-19 (2002).
48. S. Kühl, A. Tarasov, S. Zander, I. Kasatkin, and M. Behrens, Cu-Based catalyst resulting from a Cu,Zn,Al hydrotalcite-like compound: A microstructural, thermoanalytical, and in situ XAS study, *Chem. Eur. J.*, **20**, 3782-3792 (2014).
49. J. Schumann, A. Tarasov, N. Thomas, R. Schlögl, and M. Behrens, Cu,Zn-based catalysts for methanol synthesis: On the effect of calcination conditions and the part of residual carbonates, *Appl. Catal. A*, **516**, 117-126 (2016).
50. A. Tarasov, J. Schumann, F. Girgsdies, N. Thomas, and M. Behrens, Thermokinetic investigation of binary Cu/Zn hydroxycarbonates as precursors for Cu/ZnO catalysts, *Thermochim. Acta*, **591**, 1-9 (2014).
51. G. Fierro, M. Lo Jacono, M. Inversi, P. Porta, F. Cioci, and R. Lavecchia, Study of the reducibility of copper in CuO-ZnO catalysts by temperature-programmed reduction, *Appl. Catal. A*, **137**, 327-348 (1996).
52. M. M. Günter, T. Ressler, R. E. Jentoft, and B. Bems, Redox behavior of copper oxide/zinc oxide catalysts in the steam reforming of methanol studied by in situ X-ray diffraction and absorption spectroscopy, *J. Catal.*, **203**, 133-149 (2001).
53. T. van Herwijnen and W. A. de Jong, Brass formation in a copper/zinc oxide CO shift catalyst, *J. Catal.*, **34**, 209-214 (1974).
54. M. S. Spencer, The role of zinc oxide in Cu/ZnO catalysts for methanol synthesis and the water-gas shift reaction, *Top. Catal.*, **8**, 259-266 (1999).
55. T. Kandemir, F. Girgsdies, T. C. Hansen, K.-D. Liss, I. Kasatkin, E. L. Kunkes, G. Wowsnick, N. Jacobsen, R. Schlögl, and M. Behrens, In situ study of catalytic processes: Neutron diffraction of a methanol synthesis catalyst at industrially relevant pressure, *Angew. Chem. Int. Ed.*, **52**, 5166-5170 (2013).
56. J.-D. Grunwaldt, A. M. Molenbroek, N.-Y. Topsøe, H. Topsøe, and B. S. Clausen, In situ investigations of structural changes in Cu/ZnO catalysts, *J. Catal.*, **194**, 452-460 (2000).
57. P. L. Hansen, J. B. Wagner, S. Helveg, J. R. Rostrup-Nielsen, B. S. Clausen, and H. Topsøe, Atom-resolved imaging of dynamic shape changes in supported copper nanocrystals, *Science*, **295**, 2053-2055 (2002).
58. P. C. K. Vesborg, I. Chorkendorff, I. Knudsen, O. Balmes, J. Nerlov, A. M. Molenbroek, B. S. Clausen, and S. Helveg, Transient behavior of Cu/ZnO-based methanol synthesis catalysts, *J. Catal.*, **262**, 65-72 (2009).
59. T. Lunkenbein, J. Schumann, M. Behrens, R. Schlögl, and M. G. Willinger, Formation of a ZnO overlayer in industrial $Cu/ZnO/Al_2O_3$ catalysts induced by strong metal-support interactions, *Angew. Chem. Int. Ed.*, **54**, 4544-4548 (2015).
60. M. B. Fichtl, J. Schumann, I. Kasatkin, N. Jacobsen, M. Behrens, R. Schlögl, M. Muhler, and O. Hinrichsen, Counting of oxygen defects versus metal surface sites in methanol synthesis catalysts by different probe molecules, *Angew. Chem. Int. Ed.*, **53**, 7043-7047 (2014).
61. S. Kuld, C. Conradsen, P. G. Moses, I. Chorkendorff, and J. Sehested, Quantification of zinc atoms in a surface alloy on copper in an industrial-type methanol synthesis catalyst, *Angew. Chem. Int. Ed.*, **53**, 5941-5945 (2014).